Electrostatic contributions to site specific DNA cleavage by EcoRV endonuclease

ARTICLE *in* BIOCHEMISTRY · OCTOBER 2002

Impact Factor: 3.02 · DOI: 10.1021/bi0203051 · Source: PubMed

Electrostatic Contributions to Site Specific DNA Cleavage by *Eco*RV Endonuclease†

Nancy C. Horton,‡ Christopher Otey, Shelley Lusetti, My D. Sam, Jonathan Kohn, Amy M. Martin, Vidya Ananthnarayan, and John J. Perona*

Department of Chemistry and Biochemistry and Interdepartmental Program in Biomolecular Science and Engineering, University of California at Santa Barbara, Santa Barbara, California 93106-9510

Received April 24, 2002; Revised Manuscript Received July 16, 2002

ABSTRACT: Mutational analysis of amino acids at the periphery of the *Eco*RV endonuclease active site suggests that moderate-range electrostatic effects play a significant role in modulating the efficiency of phosphoryl transfer. Asp36 and Lys38 located on minor-groove binding surface loops approach within 7−9 Å of the scissile phosphates of the DNA. While the rates of single-site mutations removing the carboxylate or amine moieties at these positions are decreased 10^3−10^5-fold compared to that of wild-type *Eco*RV, we find that double mutants which rebalance the charge improve catalysis by up to 500-fold. Mutational analysis also suggests that catalytic efficiency is influenced by Lys173, which is buried at the base of a deep depression penetrating from a distal surface of the enzyme. The Lys173 amine group lies just 6 Å from the amine group of the conserved essential Lys92 side chain in the active site. Kinetic and crystallographic analyses of the *Eco*RV E45A mutant enzyme further show that the Glu45 carboxylate group facilitates an extensive set of conformational transitions which occur upon DNA binding. The crystal structure of E45A bound to DNA and Mn^{2+} ions reveals significant conformational alterations in a small α-helical portion of the dimer interface located adjacent to the DNA minor groove. This leads to a tertiary reorientation of the two monomers as well as shifting of the key major-groove binding recognition loops. Because the Glu45 side chain does not appear to play a direct structural role in maintaining the active site, these rearrangements may instead originate in an altered electrostatic potential caused by removal of the negative charge. A Mn^{2+} binding site on the scissile phosphate is also disrupted in the E45A structure such that inner-sphere metal interactions made by the scissile DNA phosphate and conserved Asp90 carboxylate are each replaced with water molecules in the mutant. These findings argue against a proposed role for Asp36 as the general base in *Eco*RV catalysis, and reveal that the induced-fit conformational changes necessary for active site assembly and metal binding are significantly modulated by the electrostatic potential in this region.

It has been argued that a preorganized polar active site environment is a major factor contributing to the catalytic efficiency of enzymes (*1*). By this model, the primary mechanism by which the activation energy is reduced, compared with the uncatalyzed reaction, is the presence of fixed charges located at distinct positions with respect to the reactive substrate moieties. In contrast to the nonenzymic aqueous-phase reaction, the same chemistry occurring within the confines of an evolutionarily optimized active site is thought to be faster because no energy cost to reorganize the dipoles has to be paid (*2*, *3*). The most obvious means by which charged enzyme moieties can accelerate bond-breaking and bond-making steps is by directly interacting with the substrate. However, several other mechanisms by which charged groups may exert influence can also be envisioned. Because Coulombic interactions vary inversely with only the first power of the distance between groups, charged residues may provide rate enhancement by optimizing the electrostatic potential from a distance. Additionally, fixed dipoles or charged groups could in principle also facilitate required induced-fit conformational changes which occur in the course of enzyme−substrate binding.

Here we address the role of electrostatics in the hydrolysis of DNA by the homodimeric type II restriction endonuclease *Eco*RV. As an enzyme family, the restriction endonucleases are of exceptional interest because they combine very high catalytic efficiencies ($k_{cat}/k_{uncat} \sim 10^{16}$-fold) with exquisite DNA sequence selectivities (*4*). For example, *Eco*RV is able to discriminate its cognate dyad-symmetric GAT/ATC site from noncognate sites differing by only one base pair, by a factor of 10^6-fold in k_{cat}/K_m (*5*). It has been demonstrated that DNA cleavage by *Eco*RV requires two or more divalent metal ions per active site subunit (*6*, *7*). From X-ray studies, the divalent metal ions are known to bind at three distinct sites located between the scissile and 3′-adjacent DNA phosphates, and several active site carboxylate groups (*8*, *9*). A functionally important distal site specific for Mn^{2+}

† Supported by NIH Grant GM53763 and ACS-PRF Grant 30427-G4 (to J.J.P.) and by American Cancer Society Postdoctoral Fellowship PF-98-015-GMC (to N.C.H.).

* To whom correspondence should be addressed. Telephone: (805) 893-7389. Fax: (805) 893-4120. E-mail: perona@chem.ucsb.edu.

‡ Current address: Department of Biochemistry and Molecular Biophysics, College of Medicine, University of Arizona, Tucson, AZ 85724.

10.1021/bi020305l CCC: $22.00
Published on Web 00/00/0000 PAGE EST: 9.3

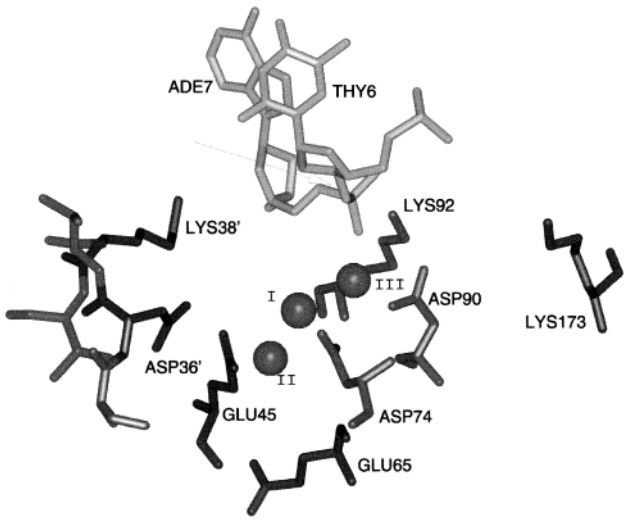

FIGURE 1: Structure of the *Eco*RV active site bound to DNA (*8*), showing the positions of positively and negatively charged amino acids relative to the scissile phosphate group. The center TA dinucleotide of the GATATC recognition site is shown in light gray, with the direction of attack by the hydroxide ion nucleophile indicated with an arrow. Lys38′ and Asp36′ emanate from the opposing subunit of the dimer. The spheres indicate the positions of divalent cations (Mg^{2+}, Mn^{2+}, or Ca^{2+}) as determined experimentally by X-ray crystallography (*8*, *9*, *11*).

cations has also been found (*10*). In terms of the reaction chemistry, it appears that the metal ions may be involved in generating the catalytic hydroxide ion nucleophile, in helping to dissociate a second water molecule for leaving group protonation, and in stabilizing the incipient negative charge in the pentacovalent transition state (*8*, *9*, *11*). The divalent metals also contribute to sequence specificity, because their affinity for the enzyme−DNA complex is substantially greater at cognate than at noncognate sites (*5*). Finally, the magnitude of the association constant for specific DNA is also enhanced by divalent metals. This is likely due to the ability of metals to shield adjacent active site carboxylate groups and DNA phosphates from each other (*12*). The central catalytic role of divalent metals together with a highly charged interface between the two macromolecules thus clearly points to a dominating influence of electrostatics in all aspects of the *Eco*RV reaction mechanism. On the basis of sequence and structure comparisons, it is clear that the importance of electrostatic interactions in providing binding complementarity and reaction rate enhancement is general to all restriction endonucleases (*4*).

Although *Eco*RV has been studied extensively by mutagenesis, enzymology, and X-ray crystallography approaches, the precise reaction mechanism remains unresolved. Two closely related mechanistic proposals, consistent with most biochemical data, invoke a transition-state model featuring three distinct divalent metal ions (Figure 1; *9*, *13*). However, a weakness of these models is that all three divalent metal sites have not been simultaneously observed in any structure (*13*). Thus, although there is broad agreement about the importance of metals and the position of at least one directly on the scissile phosphate, what is still missing is a satisfying three-dimensional description of the near-attack conformation which precisely places all metals, and in which hydroxide ion is poised to attack in-line at the tetrahedral ground-state scissile phosphate. In the absence of this, multiple interpretations of mutagenic data are more difficult to resolve. Thus, another model was recently advanced suggesting that the two carboxylate groups of Glu45 and Asp36 located 7−9 Å from the scissile phosphates together play a key role as the catalytic base (*14*). Although this model does not explain the roles of three other crucial charged side chains located closer to the scissile bond, the possibility of rearrangements in the active site en route to the transition state requires that it be carefully further assessed.

Here, we evaluate the roles of positively and negatively charged active site amino acids by mutagenesis coupled to single-turnover reaction kinetics and X-ray crystallography. Through the use of double substitutions, it is shown that Asp36 is unlikely to play a role as a catalytic base, since mutants lacking this group retain up to 2% of wild-type activity. However, these multiple mutants do reveal a very significant role for Asp36 and the adjacent Lys38 in modulating the electrostatic environment of the active site. Mutant enzymes lacking both charged groups are enhanced in activity by up to nearly 500-fold, compared with single mutants in which the electrostatic charge is apparently unbalanced. A likely electrostatic role for the nearby buried Lys173 side chain is also demonstrated. Finally, we show by crystallography that the global quaternary structure, the duplex DNA conformation, and the metal-binding sites in the partially active E45A mutant are rearranged compared to those in the wild-type enzyme. This suggests that the active site electrostatic potential contributes to catalysis by influencing the precise positioning of enzyme and substrate groups in the near-attack conformation. Together, these data also place important further constraints on the reaction mechanism of *Eco*RV.

MATERIALS AND METHODS

Preparation of EcoRV Endonuclease Mutants. Oligonucleotides were purchased from IDT (Coralville, IA), and enzymes were purchased from New England Biolabs except where noted. The K38M, K38A/D36N, and K38M/D36N mutants were constructed using a PCR-based mutagenesis protocol, as previously described for K38A (*12*). The other six mutants were constructed by site-directed mutagenesis using the QuickChange methodology (Stratagene), in which highly efficient selection for mutants derives from cleavage of methylated parental plasmid strands by *Dpn*I, leaving the newly synthesized and unmethylated mutant strands intact. The template for each mutagenesis consisted of a mixture of the expression plasmid *p*BSRV encoding the wild-type *Eco*RV gene together with an ampicillin resistance marker (*15*), and the *p*MetB plasmid encoding the *Eco*RV methyltransferase and kanamycin resistance genes (*16*). For all mutants, plasmid DNA was isolated from transformants and the sequences of the genes were verified in their entirety.

Purifications of Enzymes and DNA Substrates. Wild-type and mutant *Eco*RV enzymes were expressed in *Escherichia coli* strain MM294 (*endI*$^-$, *pro*$^-$, *thi*$^-$, $r_k^-m_k^+$), purified to homogeneity by a two-column procedure, and stored at high concentrations as an ammonium sulfate slurry, as described previously (*17*, *18*). No modifications to the purification protocol were necessary for any of the mutants. The purity of the enzymes is estimated to be ≥99% based on analysis of Coomassie-stained polyacrylamide gels. Substrate DNA

oligonucleotides comprised the wild-type non-self-complementary 16-mer 5′-GGGAAAGATATCTTGG and its complement. The DNA used in cocrystallizations is the self-complementary 11-mer 5′-CAAGATATCTT, with 5′-C overhangs. All oligonucleotides were purified by HPLC, and were lyophilized and stored at −20 °C until they were ready for use.

Enzyme Kinetics. [γ-^{32}P]ATP (6000 Ci/mmol) was purchased from Amersham. Each strand of the DNA substrate was 5′-end-labeled, purified, and annealed as described previously (*13*, *18*). Cleavage at the *Eco*RV site was assayed at 37 °C under single-turnover conditions. The enzyme and 5′-end-labeled DNA were combined at a molar ratio of 6:1 (900 and 150 nM, respectively, for all mutants except K173A, where 1350 and 225 nM, respectively, were used). These conditions ensured DNA substrate saturation at pH 7.5, as verified in control experiments at varying concentrations for each mutant. The reaction mixtures were preincubated at 37 °C in assay buffer [50 mM HEPES (pH 7.5), 100 mM NaCl, 200 mg/mL BSA, and 1 mM DTT] for 5 min. The reactions were initiated by addition of $MgCl_2$ or $MnCl_2$ to a final concentration of 10 or 2.5 mM, respectively, and the ionic strengths of all reactions were adjusted to a constant level of 140 mM using a conductivity meter. The chemical step for restriction endonuclease cleavage of DNA is known to be relatively insensitive to ionic strength (*19*). Aliquots were mixed with quench solution [8 M urea and 50 mM EDTA (pH 8.0)] at specific time points. The wild-type enzyme and E65A mutant were assessed using a rapid quench kinetics apparatus (Kintek RQF-3); in these reactions, Mg^{2+} was included in each of the two separate syringes containing either enzyme or DNA. Reaction products were separated on 8 M urea, 20% polyacrylamide gels and visualized by autoradiography, as previously documented (*13*, *18*). Rate constants were determined by fitting the data to a first-order exponential function. Under these experimental conditions, the enzyme remains fully active for reactions up to 120 h in length (*18*).

Crystallization and X-ray Structure Determination. For cocrystallization trials, the 11-mer DNA (5′-CAAGATATCTT) was brought to a concentration of 10 mg/mL (1.4 mM) in 50 mM Tris (pH 7.5) and 1 mM EDTA. Cocrystals of *Eco*RV E45A complexed with this DNA were grown by vapor diffusion at 17 °C from solutions containing 20% PEG 4K, 0.15 M sodium potassium tartrate, and 0.1 M HEPES (pH 7.5) (final conditions). The protein was prepared by resuspending the ammonium sulfate slurry at 30 mg/mL (0.5 mM) in a buffer containing 10 mM HEPES (pH 7.5), 250 mM NaCl, 1 mM EDTA, and 0.1 mM DTT, followed by exhaustive dialysis against this buffer.

A crystal of *Eco*RV E45A bound to DNA was soaked for 12 h in mother liquor supplemented with 50 mM $MnCl_2$, and cryoprotected with a solution of 25% PEG 4K, 100 mM HEPES (pH 7.5), 300 mM NaCl, and 30% glycerol, followed by flash-freezing in a stream of nitrogen gas at 100 K. X-ray diffraction amplitudes were measured on an R-AXIS IIC area detector mounted on a Rigaku RU-200 rotating anode generator. Determination of the orientation matrix, integration, scaling, and merging of data were performed with MOSFLM (*20*). The structure was phased using a previously determined *Eco*RV−DNA cocrystal structure determined in space group *P*1 (1RVA), with all solvent molecules and the side chains of Lys92, Asp90, Asp74, Glu45, Asp36, and Lys38 removed from the initial model to reduce bias. Structure determination consisted of eight rounds of model rebuilding iterated with rigid-body, positional, individual *B*-factor, and simulated annealing refinement, and was performed with the program XPLOR (*21*). Criteria for the inclusion of water molecules were the appearance of peaks at 1.0σ in $2F_o - F_c$ maps, 3.0σ in $F_o - F_c$ maps, and at least one hydrogen bonding interaction with protein or DNA. All water molecules and side chains possessing *B*-factors above 50.0 Å^2 were carefully examined prior to inclusion in the final model. Model building utilized the program CHAIN (*22*).

RESULTS AND DISCUSSION

The structure of the *Eco*RV active site shows that eight positively or negatively charged amino acids are located within 12 Å of the scissile phosphate in each subunit: Asp90, Asp74, Lys92, Glu45, Asp36, Lys38, Lys173, and Glu65 (Figure 1). It is of interest that while six of the side chains are from a single monomer, Asp36 and Lys38 emanate instead from the opposite subunit of the homodimeric enzyme. The importance of thoroughly studying the functional consequences of mutations in these side chains is highlighted by the fact that crystal structures of substrate and product complexes have so far not produced a satisfying stereochemical description of the mechanism. Given the intrinsic flexibility of DNA as well as that of the charged side chains and surrounding protein structure (*17*, *23*, *24*), it is not difficult to envision many different possible configurations of the active site in the catalytic transition state. Mutagenesis can place important constraints on possible mechanisms by ruling out the direct involvement of particular amino acids as central players in facilitating DNA hydrolysis.

Primary Catalytic Residues. Asp90, Asp74, and Lys92 are three of the most important catalytic residues in *Eco*RV. This conclusion is based primarily on three sets of experimental data. First, crystal structures of the specific *Eco*RV−DNA complex in four different crystal lattices show that these three side chains are closest to the scissile phosphate groups, with the Asp90 and Asp74 carboxylates chelating a divalent metal ion (site III, Figure 1) which forms a bridge to the scissile phosphate (*8*, *23*, *24*). Asp74 also chelates divalent metal ions bound at sites I and II (Figure 1). Second, these three amino acids are the only active site groups conserved among a subset of type II restriction endonucleases which possess the signature sequence PD...(D/E)XK (*4*). Importantly, ternary complex structures of a number of the other enzymes possessing this motif reveal that the positions of the side chain groups and scissile phosphates are superimposable with each other and with *Eco*RV (*4*), and that the metal ions in several of the other structures are appropriately positioned to facilitate conventional two-metal ion catalytic mechanisms (*25*, *26*). Mutational studies in several other type II enzymes, including *Bam*HI, *Pvu*II, and *Mun*I (*27*−*29*), have shown that removal of any of the three groups greatly attenuates DNA hydrolysis. Third, mutation of Asp90, Asp74, and Lys92 to alanine in *Eco*RV also produces enzymes with catalytic activities reduced by approximately 10^5-fold (*30*, *31*; Table 1).

While Asp90 and Asp74 each are crucial due to their role in chelation of the divalent metals, the function of Lys92 is

Table 1: Kinetic Analysis of Wild-Type and Mutant *Eco*RV Enzymes

mutant	k_{chem} (min^{-1}) (Mg^{2+})[a]	k_{chem} (min^{-1}) (Mn^{2+})	Mn/Mg[c]
wild type[b]	36 ± 4	246 ± 12	6.8
D36A	$(6.7 \pm 0.9) \times 10^{-3}$	$(5.4 \pm 0.3) \times 10^{-2}$	8.1
D36N	$(3.0 \pm 0.1) \times 10^{-3}$	$(9.3 \pm 0.02) \times 10^{-3}$	3.1
K38A	$(6.7 \pm 0.7) \times 10^{-3}$	0.2 ± 0.005	29.8
K38M	$(2.3 \pm 0.4) \times 10^{-2}$	0.5 ± 0.01	21.7
K38A/D36N	$(5.5 \pm 1.1) \times 10^{-2}$	1.4 ± 0.06	25.4
K38M/D36N	0.3 ± 0.02	4.4 ± 0.1	14.7
E45A	$(2.4 \pm 0.6) \times 10^{-3}$	0.1 ± 0.001	41.6
E65A	7.8 ± 1.8	72 ± 7.8	9.2
K173A	$(6.4 \pm 1.3) \times 10^{-4}$	1.2 ± 0.2	1875
K173M	$(3.6 \pm 0.6) \times 10^{-2}$	1.3 ± 0.1	36
K92A	1.2×10^{-3}	1.6×10^{-3}	1.3

[a] All k_{chem} values with the exception of K92A are the result of at least three determinations, and the error is reported as the standard deviation from the mean. In all cases, the rates of cleavage of the two strands were identical within experimental error. [b] Parameters for the wild-type enzyme are taken from ref *12*. [c] Mn/Mg indicates the ratio of rate constants k_{chem} for Mn^{2+}- and Mg^{2+}-dependent reactions.

less clear. Crystal structures show that the Lys92 amine is positioned on the same face of the scissile phosphate which is attacked by hydroxide ion to initiate cleavage (Figure 1; *8*, *9*). Thus, it is unlikely to preferentially bind and stabilize the pentacovalent phosphate in the transition state, as the nonesterified oxygens must move away from the amine group as the reaction progresses. Two possibilities have been suggested for the role of Lys92 depending on its protonation state. First, as a positively charged group, it may help stabilize and orient a metal-generated hydroxide ion for nucleophilic attack (*9*). Second, the pK_a of the amine may be lowered sufficiently for it to function as a catalytic base to accept a proton from the attacking water. The finding that the reaction chemistry proceeds optimally at a relatively high pH of 8.5 supports the notion that Lys92 may be the catalytic base (*13*). To distinguish between these possibilities, we attempted to reconstitute the activity of the K92A mutant by adding a set of amine compounds varying in basicity to the reaction buffers. If the reconstitutions are possible, then a linear variation of reaction rate with basicity would provide good evidence that the Lys92 amine is indeed the catalytic base, as was shown by this approach for aspartate aminotransferase (*32*). However, none of the amine compounds were able to reconstitute activity to a significant degree, even at very high concentrations (data not shown). Possibly, the extensive induced-fit rearrangements necessary for catalysis by *Eco*RV render a buffer rescue approach untenable in this case.

Further evidence in support of a central role for Asp90, Asp74, and Lys92 is that none of the mutants lacking these side chains is active in the presence of Mn^{2+} (*30*; Table 1). Because Mn^{2+} is a "soft" metal which interacts with enzyme groups via polarizable d-orbitals, it is likely to have a less stringent requirement for precise inner-sphere ligand geometry than Mg^{2+}. This in turn should allow for greater tolerance to variation in the relative positions of the scissile DNA phosphates with active site carboxylates (*10*), providing a means by which subtly altered active site structures caused by protein mutations could be offset. Indeed, there is precedent for the ability of Mn^{2+} to significantly reconstitute low Mg^{2+}-dependent activities caused by mutations in the DNA-binding cleft of *Eco*RV as well as in other restriction

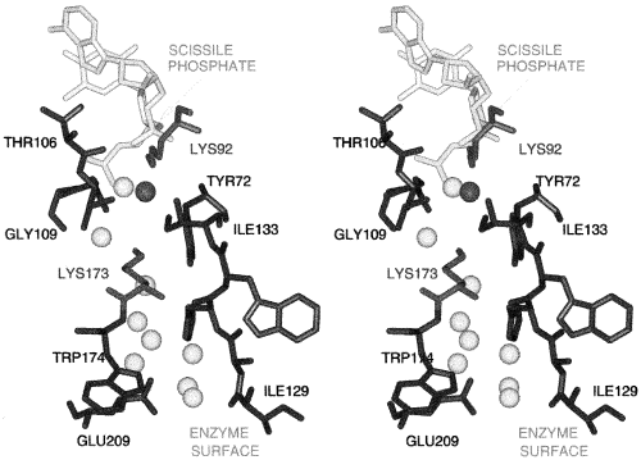

FIGURE 2: Location of Lys173 with respect to the DNA scissile phosphate. The unusual channel penetrating from the distal enzyme surface (bottom) is formed by amino acids Ile129−Ile133 and Tyr72 (right) and Thr106−Gly109 (left). The surface of the channel is partially closed by the side chains of Glu209 and His131, which approach to within 4.5 Å of each other. Exchange of the buried water molecules (spheres) with bulk water appears to be possible, however. The buried Lys173 side chain emerges at the base of the channel, entering the active site adjacent to Lys92 and the DNA scissile phosphate. The dark sphere indicates a water molecule that bridges the amine moieties of Lys173 and Lys92.

enzymes (*29*, *33*, *34*). If it is assumed that the reaction mechanism and pre-transition-state configuration are qualitatively identical in the presence of either metal ion, reconstitution of mutant function by Mn^{2+} suggests that the side chain in question is not directly involved in substrate−cofactor interactions but instead plays a more structural role. In contrast, the lack of improved Mn^{2+}-dependent cleavage by K92A, D74A, or D90A (*30*) suggests instead that these side chains are indeed central to providing rate enhancement.

A Catalytic Role for Lys173. The side chain of Lys173 is buried in the core of the protein inside of a deep narrow channel which penetrates from the surface of the enzyme at a position distant from the DNA-binding cleft (Figure 2). The channel contains a chain of water molecules which are hydrogen-bonded to each other and to protein groups. The side chain ϵ-NH_2 group of Lys173 is located at the base of the channel, and is positioned adjacent to several other waters. Strikingly, the channel extends through the protein core and terminates directly in the active site. At its base, the water molecules hydrogen-bonded to Lys173 connect the side chain nitrogen with that of the catalytically essential Lys92 near the scissile phosphate of the DNA. As Lys173 is buried, the potential exists for a lowering of its pK_a, as might be expected for a lysine residue functioning as a general base catalyst. These observations from the crystal structure raise the possibility that Lys92 and Lys173 might function together as a catalytic dyad to activate a water molecule for attack on the scissile phosphate. The function of lysine as a general base (with the accompanying decrease in pK_a) is well-described for members of the enolase superfamily (*35*), as well as for reactions involving a covalent Schiff base intermediate.

To test this possibility suggested by the structure, Lys173 was mutated to alanine and to methionine. The mutant enzymes were purified to homogeneity, and their catalytic efficiencies were tested in the presence of either Mg^{2+} or

Mn^{2+} cations. The single-turnover reaction rates show that replacement of Lys173 with alanine reduces the rate of the Mg^{2+}-dependent chemical step by 60000-fold (Table 1), a decrease comparable to that observed for enzymes mutated at Lys92, Asp90, or Asp74 (*30*; Table 1). However, the K173M mutant is improved by 60-fold compared to K173A, suggesting that at least part of the catalytic deficit is due to structural perturbations arising from removal of the hydrophobic portion of the side chain. Further, both mutants are significantly reconstituted by replacing the Mg^{2+} cofactor with Mn^{2+} ions. Indeed, the activity of K173A is increased by nearly 2000-fold in the presence of manganese, a magnitude of reconstitution significantly greater than those for most other *Eco*RV mutants (*15*). The Mn^{2+}-dependent activities of K173A and K173M are decreased by only 200-fold compared with that of the wild-type enzyme. This suggests that Lys173 is likely not a central player in the catalytic reaction. However, since it is located only 6 Å from the Lys92 amine group and 8 Å from the scissile phosphate, the significant effects of the mutations suggest that a role in facilitating the reaction through moderate-range electrostatic effects is possible. A structural role for this side chain is also likely. It is important to note that the kinetic parameters that were measured (Table 1) are single-turnover rate constants obtained at saturating substrate and metal ion concentrations, with enzyme in molar excess. These measurements specifically isolate the chemical step of the reaction apart from binding and product dissociation, allowing inferences to be made regarding factors relevant only to enhancing the phosphoryl transfer reaction.

Glu65 is an additional active site charged group whose functional role has previously not been examined by mutagenesis. The carboxylate of Glu65 is located approximately 12−13 Å from the scissile phosphate. Although this is significantly farther than Lys173, Asp36, or Lys38, Glu65 nevertheless interacts through a water molecule with a divalent metal ion bound in site II (Figure 1; *8*, *9*). Unlike the behavior of the other mutants studied here, however, single-turnover kinetics of the E65A enzyme show that the Glu65 carboxylate does not play an important role in the reaction mechanism. DNA cleavage rates are reduced by only 3−5-fold for reactions performed with either Mg^{2+} or Mn^{2+} cofactors (Table 1). The small decreases may be due to a slight destabilization of metal ion binding and/or minor electrostatic effects. The ratio of Mn^{2+}- to Mg^{2+}-dependent rates for E65A is very similar to that of the wild-type enzyme.

Asp36 and Lys38 Modulate the Active Site Electrostatic Environment. The side chains of Asp36 and Lys38 are located at the periphery of the active site some 8−10 Å from the scissile phosphate, and emanate from the opposing subunit of the dimer (Figure 1). They are poorly ordered in some crystal structures of the unliganded and DNA-bound enzyme (*17*). Mutational studies have previously suggested important roles for each of these amino acids (*14*, *36*), and we have confirmed these findings (Table 1). The decrease in the level of Mg^{2+}-dependent catalysis is 5000-fold for K38A and 1500-fold for K38M, in good agreement with the 1000-fold decrease previously found for the former mutant (*36*). A small part of this decrease may be due to a structural effect, since each of these mutants is significantly better reconstituted by Mn^{2+} ions than is wild-type *Eco*RV (Table 1).

Mutations of Asp36 cause similar or greater decreases in the catalytic rate compared with those at Lys38, and interestingly, catalysis by these mutants is not improved by Mn^{2+} ions to an extent greater than that for the wild type (Table 1). The 5000−12000-fold decreases observed for Mg^{2+}-dependent catalysis by D36A and D36N are similar to those reported for cleavage of plasmid substrates by these mutants (*14*). In the previous work, the D36E mutant was also studied and was found to retain significantly more activity than either D36A or D36N. The pH dependence of the catalytic rate for D36E suggested a significant change in the enzyme mechanism; instead of two ionizations over the range of pH 6−8 observed for wild-type *Eco*RV, the D36E mutant exhibited only one. It was thus proposed that D36 might function (together with Glu45) as a catalytic base to deprotonate water (*14*).

Although the change in the pH dependence of D36E compared to that of wild-type *Eco*RV is intriguing, other interpretations of these data are also possible. Moreover, the assignment of Glu45 and Asp36 as primary catalytic groups leaves the greater effects caused by the Asp90, Asp74, and Lys92 mutants unexplained. Further, a separate study of the pH dependence of the catalytic step by our laboratory gave very different results, showing a sharp bell-shaped curve with only a single ionization on the acidic limb and a high pH optimum of 8.5 (*13*). Therefore, to further explore the role of Asp36, we combined the D36N mutation at this position with mutants of Lys38 to produce the K38A/D36N and K38M/D36N double mutants. Kinetic analysis of these enzymes shows that their catalytic rates are improved over the rates of each of the four single mutants, under both Mg^{2+}- and Mn^{2+}-dependent catalytic conditions. Most strikingly, the addition of the K38M mutation to D36N improves the rate of the chemical step in the latter mutant by nearly 500-fold. With Mn^{2+} as a cofactor, the K38M/D36N double mutant is reduced in activity by only 55-fold compared with wild-type *Eco*RV. This rate is also approximately 10-fold greater than that observed for the K38M mutant enzyme (Table 1).

The reconstitution of activity in the Asp36/Lys38 double mutants strongly suggests that Asp36 is not likely to perform as the catalytic base in DNA cleavage by *Eco*RV, as was previously suggested (*14*). Instead, the analysis reveals that these side chains play a subsidiary role in promoting the catalytic activity of the enzyme, most likely by modulating the electrostatic potential within the active site cleft. Mutants in which either the negatively charged Asp36 carboxylate group or the positively charged Lys38 amine has been removed apparently possess an unbalanced charge distribution in the vicinity of the scissile phosphodiester bond. The rebalancing of the electrostatic potential via substitution of the remaining charged group then results in substantial improvements in catalytic rate. This double mutant analysis may provide an important general approach toward elucidating the function of longer-range electrostatic forces in enzyme catalysis. We are unaware of prior experiments in which multiple mutants have been used to demonstrate such a role.

The structure of *Eco*RV shows that Asp36 and Lys38 are positioned to most directly influence the catalytic activity

Table 2: Crystallographic Data Collection and Refinement Statistics for the *Eco*RV E45A−DNA−Mn^{2+} Complex

DNA sequence	resolution (Å)	space group	cell dimensions						% data coverage[a]	R_{merge}[e]	B_{over} (Å^2)[b]	R_{cryst}[c]	R_{free}[f]	rmsd for bonds (Å)	rmsd for angles (deg)	no. of waters
			a (Å)	*b* (Å)	*c* (Å)	α (deg)	*β* (deg)	*γ* (deg)								
CAAGATATCTT[d]	1.9	*P*1	47.9	48.7	63.7	96.8	109.6	106.7	90	0.069	27.8	0.214	0.306	0.014	1.98	281

[a] Includes all data in the intensity range of $I/\sigma(I) > -3.0$. [b] The overall *B*-factor is determined from a Wilson plot of the structure factor data using a low-resolution cutoff of 4.0 Å. [c] $R_{cryst} = (\sum_h \sum_i ||F_{obs}| - |F_{calc}||)/(\sum |F_{obs}|)$, where F_{obs} and F_{calc} are the observed and calculated structure factor magnitudes, respectively. Refinement was carried out using a low-resolution cutoff of 5.0 Å. [d] The following residues were not modeled: R144 in subunit I, K98−E101, V141−S146 in subunit II, and C1 in DNA strand I. The following side chains were truncated following the *β*-carbon: K17, K38, E57, K58, I62, K67, K98, E99, N100, K104, R140, K145, K149, K203, S223, Q224, N227, and N228 in subunit I and K17, K38, K67, K85, K104, N116, R140, K149, N154, K197, K203, and L225 in subunit II. [e] $R_{merge} = (\sum_h \sum_i |\langle F_h \rangle - F_{hi}|)/(\sum_h F_h)$, where $\langle F_h \rangle$ is the mean structure factor magnitude of *i* observations of symmetry-related reflections with Bragg index *h*. [f] R_{free} is calculated with removal of 10% of the data as the test set, followed by simulated annealing refinement of the final model.

of the opposing subunit of the monomer (Figure 1), and this appears to be the most likely means by which the mutational effects make themselves felt. This inference based on the crystal structure was contradicted by experiments involving heterodimers of *Eco*RV with mutant and wild-type subunits, from which it was concluded that both Asp36 and Lys38 affect the catalytic activity only within their own subunit (*36*, *37*). However, it is possible that the preparations of wild-type−mutant heterodimers required for these experiments may be contaminated by small amounts of wild-type−wild-type or mutant−mutant homodimers.

Catalytic Role of Glu45. The importance of Glu45 was suggested by the initial crystal structures of *Eco*RV (*23*) and by early mutagenesis experiments (*30*), which showed that the E45A mutant is compromised by some 10^4-fold compared to the wild-type enzyme. Glu45 is located approximately 8 Å from the scissile phosphate and ligates a divalent cation bound in site II (Figure 1). The activity of E45A is reconstituted to some extent by Mn^{2+} ions (Table 1; *31*), showing that metal binding to other active site carboxylates is sufficient for catalysis, albeit at levels that remain 2500-fold below those of the wild-type enzyme. Thus, the mutagenesis data suggest that Glu45 has a more direct role in catalysis than Lys173, Lys38, or Asp36, but is less central than Lys92, Asp90, or Asp74. This gradation in mutant activity corresponds approximately with the relative positions of the side chain and the scissile DNA phosphate, with the most proximal Lys92, Asp90, and Asp74 groups causing the greatest decreases in catalytic rate when mutated. Taken together, the mutagenesis data support the notion that the scissile phosphate does not move far from the position observed in crystal structures, to reach the conformation in which the nucleophile is poised to attack.

While some precise detail has yet to be elucidated, it thus appears that Lys92, Asp90, and Asp74 are most central and directly involved in the rate enhancement, while Lys173, Lys38, and Asp36 have supporting electrostatic or structural roles. However, the role of Glu45 remains the most obscure. To provide further insight into the role of Glu45 in catalysis, we therefore examined the structural consequences of replacing the glutamate side chain with alanine by X-ray crystallography. We wished to obtain the structure of a mutant ground-state uncleaved complex in the presence of a metal ion which supports catalysis. To accomplish this, *Eco*RV E45A was cocrystallized with DNA in the absence of metals, under conditions similar to those previously employed for wild-type and modified binary and ternary complexes (*8*, *11*, *17*). Large crystals of the E45A−DNA complex were then soaked in solutions of mother liquor and cryoprotectant supplemented with 50 mM $MnCl_2$, and a data set was measured to 1.9 Å resolution at 100 K (Table 2). The refined structure reveals clear and continuous electron density across both scissile phosphates, demonstrating that a precleaved ground-state complex has been trapped (Figure 3). The lack of enzyme activity observed in this soaking experiment is consistent with findings from similar studies of the wild-type enzyme, which showed that *Eco*RV is not catalytically active in this crystal lattice environment (*8*).

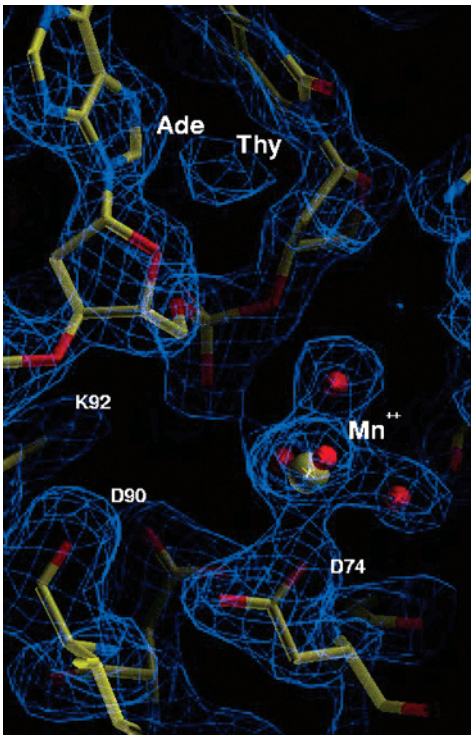

FIGURE 3: Simulated annealing omit map in the region of the active site. The map is displayed at a contour of 1.0σ. The manganese ion and water sphere, the center dinucleotide step of the DNA, and enzyme residues Lys92, Asp90, Asp74, and Glu45 were removed from the model prior to performing a simulated annealing protocol in XPLOR (*19*).

Comparison of the wild-type and *Eco*RV E45A structures shows that the mutation causes large-scale conformational rearrangements in the enzyme (Figure 4a). The *Eco*RV dimer possesses a modular structure in which the two DNA binding/catalytic domains and the dimer interface each move as rigid bodies upon binding of DNA (Figure 4b; *17*). Compared to wild-type *Eco*RV, in E45A the two DNA-binding domains are rotated apart by 2.6° about an axis roughly perpendicular

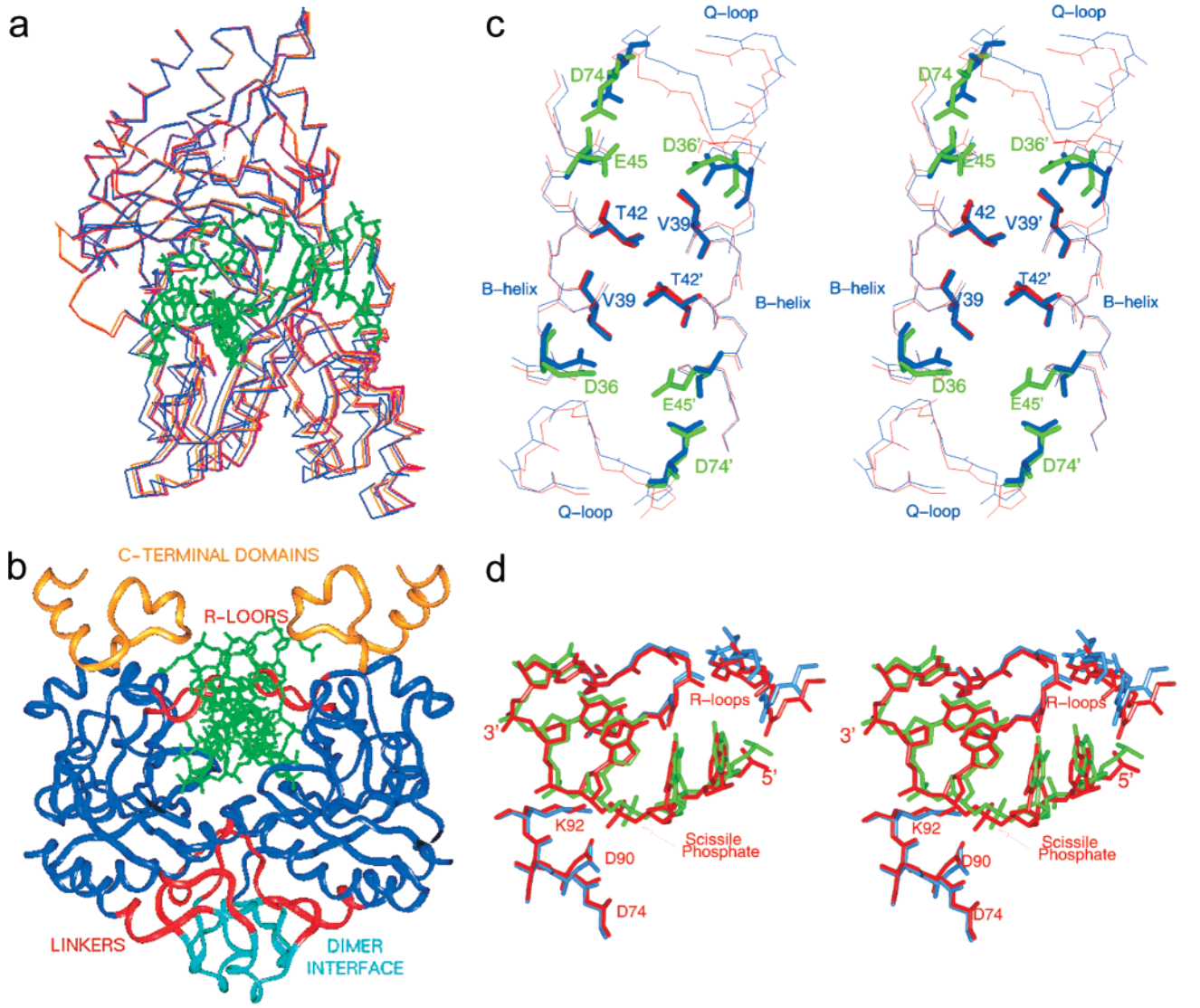

FIGURE 4: (a) Quaternary structure differences among three wild-type *Eco*RV structures and the E45A mutant. α-Carbon backbone traces are shown for E45A (blue) and wild-type *Eco*RV: the binary specific complex [red (*8*)], the binary complex soaked in Mg^{2+} ions [orange (*8*)], and the ternary specific complex cocrystallized with Ca^{2+} ions [purple (*16*)]. The structures are superimposed using backbone atoms in the core domains of subunit II (top), showing the divergence in subunit I domain orientation in the mutant (bottom). The duplex DNA in green is from the E45A mutant complex. (b) Diagram of the *Eco*RV−DNA crystal structure (*8*) showing the modular enzyme design. The DNA binding and/or catalytic subunits are in dark blue. (c) Stereoview of a superposition of *Eco*RV E45A (blue) and wild-type *Eco*RV (red) derived from the ternary complex with specific DNA and Mg^{2+} ions (*8*). Key side chains D74, E45, and D36 from each subunit of the wild-type enzyme are in green. The superposition is based on backbone atoms of amino acids Val39−Thr42 and Val39′−Thr42′. (d) Stereoview of a superposition of E45A (blue and green) and wild-type *Eco*RV (red) structures based on backbone atoms in the core domain of subunit II (rms deviation = 0.27 Å). Asp90, Asp74, and Lys92 of subunit II are shown at the bottom. The shifted position of the DNA scissile phosphate bound in this subunit is evident. Alterations in the relative positions of the R loops (top) are also clear. The R loop of subunit II is at the left, and that of subunit I is at the right.

to the DNA-binding cleft. The internal structures of the rigid portions of each individual DNA-binding subunit, which comprise 122 amino acids located mainly in core secondary structure elements (*17*), are unchanged. A similar although somewhat smaller reorientation of domains by 1.8° was also observed in the *Eco*RV T93A−DNA mutant complex (*9*).

Careful superposition of three independent structures of the wild-type *Eco*RV−DNA−Mg^{2+} ternary complex (Figure 4a; *8*, *17*) with that of E45A suggests that the global conformational change has its origins in altered electrostatic interactions near a small dimer interface formed by the amino termini of the enzyme B-helices. The two B-helices run antiparallel in the DNA minor groove, with the side chains of Val39 and Thr42 from each monomer interdigitating to form the intersubunit packing contacts. Superposition of the protein backbones at Val39−Thr42 in both subunits (rms deviation = 0.22 Å) shows that the structure of this small interface is not influenced by the E45A substitution (Figure 4c). However, the positions of the nearby Asp74 and Asp36 side chains are significantly altered. The changes are more marked in subunit I (Figure 4c, top) than in subunit II, as is also revealed by superpositions performed on each B-helix separately. Very similar structural changes can be noted when E45A is superimposed with the binary wild-type complex (*8*) as well as with the ternary wild-type complex cocrystallized with Ca^{2+} ions (*17*), each in the same crystal lattice. Thus, the observed rearrangements are due to the mutation and do not arise from either the presence of a divalent metal

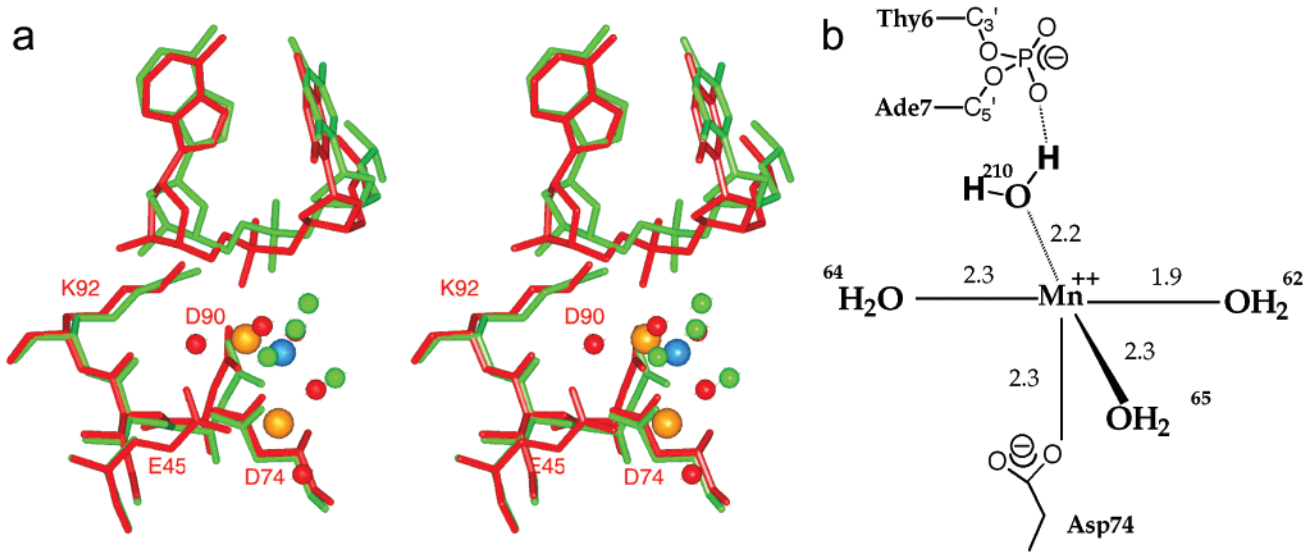

FIGURE 5: (a) Comparison of the position of the Mn^{2+} ion found in the active site of E45A (green) with those of the Mg^{2+} ions previously located in the crystal structure of the wild-type complex (*8*). The superposition was performed as described for Figure 4d. The larger orange spheres represent Mg^{2+} ions bound in sites II and III in the wild-type complex, and the larger blue sphere represents the Mn^{2+} ion bound in E45A. The smaller red and green spheres represent metal-associated waters in the wild-type (red) and E45A (green) structures. (b) Diagram of the inner-sphere ligands and distances in angstroms for the Mn^{2+} ion modeled in subunit II of the *Eco*RV E45A−DNA complex.

or its identity, or from differences in crystal packing contacts.

In wild-type *Eco*RV, the side chain of Glu45 projects into each active site but does not interact closely with other protein groups. Indeed, the side chain is poorly ordered in wild-type structures unless site II (Figure 1) is occupied by a metal ion (*8*, *9*, *17*). However, no change in the global conformation of wild-type complexes occurs if this side chain is poorly ordered; only its replacement with a methyl group generates the rearrangements (Figure 4a,c). Since the Glu45 carboxylate thus apparently does not play a structural role, we suggest instead that the origin of the altered global structure in the E45A mutant is likely to be achievement of a new optimal balance of electrostatic forces. Glu45 is centrally located among the constellation of charged groups surrounding the scissile and 3′-adjacent DNA phosphates (Figure 1). Clearly, the E45A mutant is thus affected both in its possibilities for metal ion chelation and in the electrostatic potential in the active site. The repositioning of charged groups observed in the mutant structure is facilitated by the intrinsic flexibility of the protein structure in this region, which allows the motions to occur. Indeed, Asp36 bridges directly into one of the flexible linkers connecting the catalytic domain with the larger dimer interface (Figure 4b), and these linkers facilitate the adoption of altered enzyme quaternary structure. This role of the linkers is clear from many comparisons of unliganded and DNA-bound *Eco*RV structures (*17*, *23*).

The structural changes affect the positions of the Thr37 side chains as well as the orientations of the nearby "Q-loop" segments (Figure 4c), and alter some of the enzyme contacts to the sugar−phosphate backbone by these groups. Several studies have previously implicated contacts of Thr37 with the adjacent Gln69 and a DNA ribose as central to the generation of force to facilitate the required DNA bending (*23*, *38*). A set of crystal structures of the *Eco*RV−DNA complex in different crystal lattice environments showed a correlation of minor-groove surface area burial with the degree of DNA bending, suggesting a structural pathway mediated by these key Thr37 contacts (*24*). A loss of the Thr37 contact is also correlated with destabilization of metal binding in base−analogue complexes of the enzyme (*18*). Thus, the rearrangement of this region in the E45A mutant suggests that electrostatic forces play an important role in facilitating the conformational transitions necessary to precise active site assembly and metal binding.

The conformational readjustments in the mutant complex are not limited to the minor groove but also extend throughout the DNA binding cleft. Although all the specific base contacts with GATATC are preserved, the major-groove recognition loops are shifted by ~0.5 Å with respect to each other in the mutant (Figure 4d). Further, and perhaps most importantly, the scissile phosphate group in subunit II of E45A is shifted by ~1.3 Å from its position in the ternary complexes of wild-type *Eco*RV bound to metal ions. Small structural changes in the DNA backbone structure across the target site also are present in the DNA strand binding to this subunit (Figure 4d). In contrast with subunit II, the conformation of the DNA strand bound in the subunit I active site is not significantly different from the wild-type complex, and the relative positions of the scissile phosphate and active site groups are also preserved in that monomer.

Manganese Ion Binding Sites in the E45A Mutant. Manganese ions were located at four sites on the dimeric protein. Two of these sites bridge the imidazole rings of His71 in each subunit, with a DNA phosphate flanking the cleavage site. These Mn^{2+} binding sites have been documented previously (*10*, *11*). The occupancy of this site inhibits Mn^{2+}-dependent hydrolysis at cognate sites by *Eco*RV, while its removal by mutation hinders the ability of the enzyme to discriminate against a noncognate sequence. A third Mn^{2+} ion in the E45A structure appears to be ligated to His193 in one subunit, far from the active site and also as previously described (*11*). The fourth manganese ion binds in the active site in subunit II only (Figure 5a). It forms short inner-sphere interactions with four water molecules and a

fifth close contact with the side chain carboxylate group of Asp74 (Figure 5b).

The fourth binding site for a divalent cation is not occupied in any other *Eco*RV−DNA−M^{2+} cocrystal structure bound to Mg^{2+}, Mn^{2+}, or Ca^{2+} ions (*8*, *9*, *11*, *17*, *18*). It thus represents a fourth distinct position (site IV) within the *Eco*RV active site at which divalent metals may bind. Site IV is most closely related to the previously described 90/74 site (site III, Figure 1) which bridges the scissile DNA phosphate with the carboxylates of Asp90 and Asp74 (*8*). On the basis of a superposition of backbone atoms from 122 core residues within the catalytic domain (rms deviation = 0.27 Å), the Mn^{2+} ion at site IV in the E45A structure is found to be 2.3 Å from the 90/74 site occupied in crystals of wild-type *Eco*RV soaked with Mg^{2+} ions (*8*). Site IV lies between site III and the 74/45 site (site II) also bound by Mg^{2+}, and is located 3.6 Å from the latter. The Mn^{2+} ion at this position refines to an atomic *B*-factor of 48.6 $Å^2$ and appears at 4σ peak height in a simulated annealing electron density map calculated with coefficients $2F_o - F_c$, considerably higher than the peak heights of adjacent waters. Its inner ligation sphere differs from the nearby site III mainly in replacement of the Asp90 and scissile DNA phosphate contacts with water molecules.

In contrast to the results of Mg^{2+} soaks, soaking of Mn^{2+} ions into wild-type *Eco*RV−DNA cocrystals in the identical crystal lattice showed binding solely at site III of subunit II (*8*). This represents the same experimental protocol that was used to visualize Mn^{2+} binding in the E45A structure. Thus, the effect of the mutation on metal binding under nearly identical experimental conditions is to produce a 2.3 Å shift in the position of the cation. It appears that this arises primarily from the outward displacement of the scissile phosphate (Figure 4d), which increases the separation between the *pro-S* oxygen and the Asp90 carboxylate from 3.5 Å in the wild type to 4.5 Å in E45A. Thus, removal of the Glu45 carboxylate does not directly affect metal binding, because the metal which coordinates Glu45 (the site II metal) was not occupied in the wild-type complex. Instead, it is the site III metal which is rearranged as a consequence of the altered induced-fit pathway. The implications of this rearrangement for the ability of the enzyme to facilitate reaching the pre-transition-state conformation cannot be described in detail. However, the replacement of a direct metal contact to the scissile phosphate with a water-mediated interaction will decrease compensation of the additional incipient negative charge in the approach to the pentacovalent transition state. This factor alone may readily account for the 10^3−10^4-fold decrease in rate enhancement by the E45A mutant.

Conclusions. The kinetic and crystallographic analysis of charged active site mutants provides insight into how electrostatic forces operate to provide catalysis by this type II restriction enzyme. Since double mutation of Asp36 and Lys38 produces enzymes retaining relatively high activity, it appears likely that these groups do not directly interact with the scissile DNA phosphate. However, the enhanced phosphoryl transfer rate (k_{chem}) of the double compared to the single mutants clearly demonstrates an important electrostatic effect, which appears to operate over a distance of 6−10 Å. Charged groups in the active site periphery thus have important roles in stabilizing the transition state, even though they do not interact directly with the reacting substrate moiety. A general mechanism which may explain this effect is suggested by the structure of the E45A mutant, which shows global changes in quaternary structure and a consequent mispositioning of the scissile phosphate in the active site. Clearly, effects of this kind may also occur to generate decreased catalytic efficiency in the Asp36 and Lys38 mutants. Given the structural similarities among the active sites in type II restriction endonucleases (*4*), it seems likely that electrostatic effects at a distance contribute to catalysis in other enzymes as well.

This study also places some additional constraints on the reaction pathway of *Eco*RV. In particular, the weight of evidence now suggests strongly that, if significant rearrangements to the scissile phosphate do occur in the approach to the transition state, these must be such as to retain its proximity to Lys92, Asp90, and Asp74. Both the three-metal ion mechanisms previously proposed by our group (*9*, *13*) and a two-metal mechanism proposed by Halford, Winkler, and colleagues (*6*−*8*, *39*) fit within this constraint. Elucidation of a feasible structural pathway from the observed ground-state structures to the transition state required only small rearrangements in the case of the three-metal mechanism (*9*). However, a flipping of the scissile phosphate deeper into the active site, into a feasible position for a two-metal mechanism, was observed by unconstrained molecular dynamics (*39*). Which of these possibilities in fact obtains further structural evidence. Proposals for a one-metal mechanism (*31*) appear to be less tenable, because of the clear kinetic evidence implicating multiple metals (*6*, *7*), together with the lack of convincing evidence for a catalytically relevant Mg^{2+} binding site outside the immediate active site.

REFERENCES

1. Warshel, A. (1998) *J. Biol. Chem. 273*, 27035−27038.
2. Warshel, A. (1978) *Proc. Natl. Acad. Sci. U.S.A. 75*, 5250−5254.
3. Warshel, A., Sussman, F., and Hwang, J.-K. (1988) *J. Mol. Biol. 201*, 139−159.
4. Pingoud, A., and Jeltsch, A. (2001) *Nucleic Acids Res. 29*, 3705−3727.
5. Taylor, J. D., and Halford, S. E. (1989) *Biochemistry 28*, 6198−6207.
6. Baldwin, G. S., Vipond, I. B., and Halford, S. E. (1995) *Biochemistry 34*, 705−714.
7. Vipond, I. B., Baldwin, G. S., and Halford, S. E. (1995) *Biochemistry 34*, 697−704.
8. Kostrewa, D., and Winkler, F. K. (1995) *Biochemistry 34*, 683−696.
9. Horton, N. C., Newberry, K. J., and Perona, J. J. (1998) *Proc. Natl. Acad. Sci. U.S.A. 95*, 13489−13494.
10. Sam, M. D., Horton, N. C., Nissan, T. A., and Perona, J. J. (2001) *J. Mol. Biol. 306*, 851−861.
11. Horton, N. C., Connolly, B. A., and Perona, J. J. (2000) *J. Am. Chem. Soc. 122*, 3314−3324.
12. Martin, A. M., Horton, N. C., Lusetti, S., Reich, N. O., and Perona, J. J. (1999) *Biochemistry 38*, 8430−8439.
13. Sam, M. D., and Perona, J. J. (1999) *Biochemistry 38*, 6576−6586.
14. Stanford, N. P., Halford, S. E., and Baldwin, G. S. (1999) *J. Mol. Biol. 288*, 105−116.
15. Vipond, I. B., and Halford, S. E. (1996) *Biochemistry 35*, 1701−1711.
16. Vermote, C. L., Vipond, I. B., and Halford, S. E. (1992) *Biochemistry 31*, 6089−6097.
17. Perona, J. J., and Martin, A. M. (1997) *J. Mol. Biol. 273*, 207−225.
18. Martin, A. M., Sam, M. D., Reich, N. O., and Perona, J. J. (1999) *Nat. Struct. Biol. 6*, 269−277.

19. Lesser, D. R., Kurpiewski, M. R., and Jen-Jacobson, L. (1990) *Science 250*, 776−786.
20. Bailey, S. (1994) *Acta Crystallogr. D50*, 760−763.
21. Brunger, A. T., Kuriyan, J., and Karplus, M. (1987) *Science 235*, 458−460.
22. Sack, J. S. (1988) *J. Mol. Graphics 6*, 224−225.
23. Winkler, F. K., Banner, D. W., Oefner, C., Tsernoglou, D., Brown, R. S., Heathman, S. P., Bryan, R. K., Martin, P. D., Petratos, K., and Wilson, K. S. (1993) *EMBO J. 12*, 1781−1795.
24. Horton, N. C., and Perona, J. J. (2000) *Proc. Natl. Acad. Sci. U.S.A. 97*, 5729−5734.
25. Horton, J. R., and Cheng, X. (2000) *J. Mol. Biol. 300*, 1049−1056.
26. Viadiu, H., and Aggarwal, A. K. (1998) *Nat. Struct. Biol. 5*, 910−916.
27. Xu, S. Y., and Schildkraut, I. (1991) *J. Biol. Chem. 266*, 4425−4429.
28. Nastri, H. G., Evans, P. D., Walker, I. H., and Riggs, P. D. (1997) *J. Biol. Chem. 272*, 25761−25767.
29. Lagunavicius, A., and Siksnys, V. (1997) *Biochemistry 36*, 11086−11092.
30. Selent, U., Ruter, T., Kohler, E., Liedtke, M., Thielking, V., Alves, J., Oelgeschager, T., Wolfes, H., Peters, F., and Pingoud, A. (1992) *Biochemistry 31*, 4808−4815.
31. Groll, D. H., Jeltsch, A., Selent, U., and Pingoud, A. (1997) *Biochemistry 36*, 11389−11401.
32. Toney, M. D., and Kirsch, J. F. (1989) *Science 243*, 1485−1488.
33. Vipond, I. B., Moon, B.-J., and Halford, S. E. (1996) *Biochemistry 35*, 1712−1721.
34. Jeltsch, A., Alves, J., Oelgeschlager, T., Wolfes, H., Maass, G., and Pingoud, A. (1993) *J. Mol. Biol. 229*, 221−234.
35. Babbitt, P. C., Hasson, M. S., Wedekind, J. E., Palmer, D. R. J., Barrett, W. C., Reed, G. H., Rayment, I., Ringe, D., Kenyon, G. L., and Gerlt, J. A. (1996) *Biochemistry 35*, 16489−16501.
36. Stahl, F., Wende, W., Wenz, C., Jeltsch, A., and Pingoud, A. (1998) *Biochemistry 37*, 5682−5688.
37. Stahl, F., Wende, W., Jeltsch, A., and Pingoud, A. (1998) *Biol. Chem. Hoppe-Seyler 379*, 467−473.
38. Wenz, C., Jeltsch, A., and Pingoud, A. (1996) *J. Biol. Chem. 271*, 5565−5573.
39. Baldwin, G. S., Sessions, R. B., Erskine, S. G., and Halford, S. E. (1999) *J. Mol. Biol. 288*, 87−103.

BI020305L